J Mater Sci: Mater Electron (2021) 32:22408–22416

Relaxor ferroelectric-like behavior in $10PbTiO_3$–$10Fe_2O_3$–$30V_2O_5$–$50B_2O_3$ glass for energy storage applications

M. M. El-Desoky[1,2], N. K. Wally[1], A. M. Ali[1], Amany E. Harby[1], and Ahmed E. Hannora[3,*]

[1] Department of Physics, Faculty of Science, Suez University, Suez 43518, Egypt
[2] Academy of Scientific Research and Technology (ASRT) of the Arab Republic of Egypt, Cairo, Egypt
[3] Department of Science and Engineering Mathematics, Faculty of Petroleum and Mining Engineering, Suez University, Suez 43518, Egypt

Received: 19 June 2021
Accepted: 27 July 2021
Published online: 11 August 2021

ABSTRACT

Recently, demand increased for dielectric materials used in energy storage devices at high voltage applications. Appearance of polar clusters in glass matrix could promote its use in energy storage applications. Conventional quenched glass sample of composition $10PbTiO_3$–$10Fe_2O_3$–$30V_2O_5$–$50B_2O_3$ were successfully developed. The glassy nature was confirmed by XRD and DSC measurements. Boson peak observed at low frequency from the Raman spectra confirms polar cluster formation. Dielectric properties of prepared glass were investigated in a wide range of frequency and temperature. Broad and diffuse peak of dielectric permittivity shifted to the higher temperatures, denoting the typical relaxor ferroelectrics like behavior. Sample shows energy storage density of about 164.7 mJ/cm^3 at room temperature. Quenched glass sample shows typical anti-ferromagnetic behavior.

1 Introduction

Energy storage applications attracted considerable attention specially with relaxor ferroelectric materials. Relaxor ferroelectrics are a class of disordered crystals possessing unique, scale-dependent symmetry. They are distributed randomly among the equivalent lattice sites forming quenched local dipoles [1]. Relaxors were observed in perovskite structure that have randomness associated with one or more of the atoms in the unit cell. The real part of the dielectric permittivity of these materials characterized by large values with wide peak in the temperature dependence. Also, they are showing a frequency dependent behavior [2–4]. Polar nanoregions occurrence in paraelectric phase accepted to be the origin of the relaxors. Also, broken bonds with sufficient amount give rise to (weak) random dipolar fields which act as pinning centers of the thermally fluctuating polarization [4]. Few papers have been

Address correspondence to E-mail: Ahmed.Hannora@suezuniv.edu.eg

https://doi.org/10.1007/s10854-021-06727-3

reported on physical properties of lead titanate doped in borate glasses. They concluded that the dielectric constant measurements with temperature and fixed frequencies confirm ferroelectric relaxors behavior [5, 6].

Impedance spectroscopy is a powerful technique for electrical conductivity of complex charge transport materials. To distinguish charge transport processes in ceramics or glass-ceramics materials, electronic, ionic and/or mixed electronic-ionic, microstructure and impedance spectroscopy are of great importance [7]. Currently, the requirement of advanced materials with improved physical properties in potential applications are of great significance. Nano-sized materials usually exhibit superior properties than bulked similar materials [8].

In the present work, high melting temperature lead titanate and iron oxide which have a poor glass forming ability were added to the glass former and modifier, boron and vanadium oxides. The electrical properties of vanadium pentoxide glass depend on the synthesis conditions due to the changes in V^{4+}/V^{5+} ratio. Higher temperature of nanocrystalline vanadate glass led to higher conductivity enhancement, due to higher concentration of V^{4+} hopping centers [8–10]. Also, the same features were observed for Fe^{2+}/Fe^{3+} hopping [9]. The energy storage density affected by inner defects, especially oxygen vacancies. The purpose of the present work is to investigate the effect of frequency and temperature on the AC conductivity and dielectric properties of the quenched $10PbTiO_3–10Fe_2O_3–30V_2O_5–50B_2O_3$ glass within the frequency range 500 Hz to 1 MHz at various temperatures within 293–473 K. Also, the modulus behavior is investigated for the prepared glass. The structure, relaxor/ferroelectric and ferromagnetic properties of the studied sample are discussed in the situation of its ability to energy storage applications.

2 Experimental procedure

$10PbTiO_3–10Fe_2O_3–30V_2O_5–50B_2O_3$ glass is prepared by the conventional quenching method from high purity oxides > 99%, $PbTiO_3$, Fe_2O_3, V_2O_5 and B_2O_3 (Aldrich and Alfa Aesar) in porcelain crucibles at 1473 K for 30 min. The melt was poured and pressed between stainless steel plates. Dark black sample with thickness from 1.1 to 1.3 mm was formed. Thermal analysis was carried out using differential scanning calorimeter (DSC) NETZSCH DSC 204HP at heating rates of 10 K/min. Siemens D5000 X-ray diffractometer was used for structural analysis with Cu kα radiation (λ = 0.154 nm) at a scan rate of 3°/min. under accelerating voltage of 40 kV and current of 30 mA. Silver paste electrodes were deposited on both faces of the polished samples. The dielectric measurement at different frequencies in the range of 500 Hz to 1 MHz using MICROTEST 6377 LCR meter at temperatures range of 298–475 K. The polarization– electric field (P–E) hysteresis loops of the quenched glass sample were measured using a Sawyer–Tower circuit. The magnetic properties of the specimen were measured by a Vibrating Sample Magnetometer (VSM) Lake Shore model 7410 (USA). WITec confocal Raman microscope alpha 300R, Germany was conducted at room temperature for glass structure investigation in the wavelength range of 50 to 1000 cm^{-1} with a resolution of 2 cm^{-1}.

3 Results and discussion

3.1 Structural analysis

The non-crystalline nature of the glass sample was investigated by X-ray diffraction technique at room temperature, Fig. 1. The as-quenched sample show a broad hump indicating its amorphous nature. As-quenched glass sample was subjected to heating and cooling cycling test using differential scanning calorimeter (DSC). As can be seen in the heating mode there are two endothermic peaks at relativity low temperature 401 and 437 K, Fig. 2. The third endothermic was observed at 796 K which is related to milting temperature of the glass sample. Two exothermic peaks were observed, small broad one at 696 and large sharper one at 714 K related to crystallization events. During the cooling mode, only small broad exothermic peaks were observed at 711 K. The same feature was observed in Ref. [11]. The endothermic event at 666 K corresponding to the glass transition temperature. The two endothermic peaks lower than glass transition temperature are related to relaxor ferroelectrics phase formation and/or ferroelectric to paraelectric phase transition. It is concluded that, as-quenched Bi_2O_3-Pb_3O_4-CuO-K_2O glass shows unfamiliar ferroelectric behavior [11].

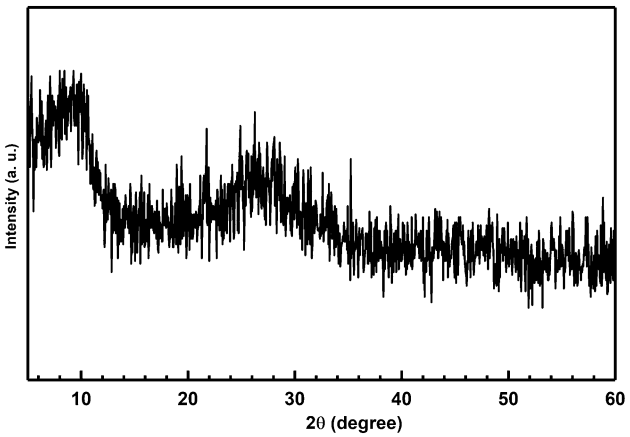

Fig. 1 XRD pattern of $10PbTiO_3$–$10Fe_2O_3$–$30V_2O_5$–$50B_2O_3$ glass

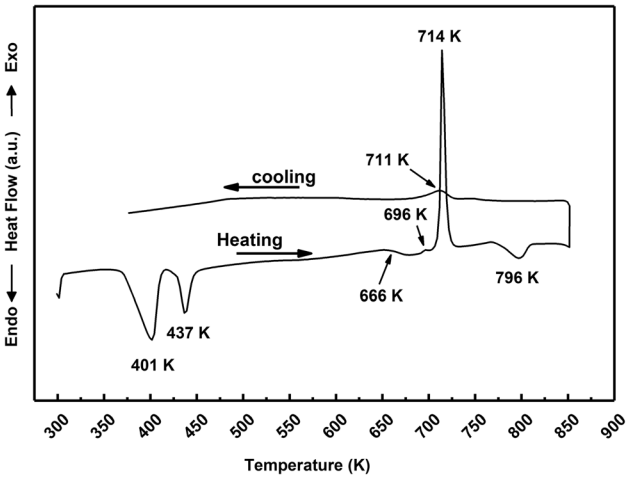

Fig. 2 DSC curves of $10PbTiO_3$–$10Fe_2O_3$–$30V_2O_5$–$50B_2O_3$ glass

According to Fig. 2 and during the cooling path the endothermic peaks completely disappeared.

The dynamics of network glasses can be investigated by relaxational or vibrational processes at short and intermediate scales of glass. In low frequency light scattering experiments, the relaxational and vibrational processes often overlap depending on the glass and temperature [12]. The glass structure was also investigated by Raman spectroscopy, Fig. 3. Boson peak at low frequency was observed from the Raman spectra. This peak is associated with the existence of intermediate range order structure in glass systems. Small fine polar clusters could be formed during the quenching process [13, 14]. The excitation exhibit at low frequency "soft mode excitation" characterize the ferroelectric transition [15]. The hump occurs at low frequency range of 30 to 180 cm^{-1} due to Boson peak and the motion of barium and lead ions against the BO_6 octahedra. Also. Broad peak from 220 to 580 cm^{-1} is related to fine clusters of V_2O_5 and stretching vibrations peak of O−Ti−O. Peak observed around 690 cm^{-1} is related to VO_6 and TiO_6 fine clusters. Stretching vibrations of B−O bonds observed at 920 due to is related to pyramidal BO_3 unit. The same results were observed and confirmed by FT-IR in our previous work [5, 6, 16]. Also, the TEM in our recent previous work of the present sample confirms plate-like sheets of micro-size, containing nanoclusters or polar nanoclusters in their structure [16].

3.2 Dielectric properties

The analysis of *AC* impedance spectra is of great value. For electrical behavior of glass sample impedance spectroscopy, the plotting of real and imaginary parts of the complex electrical quantities as a function of angular frequency (ω = 2πf, f is the frequency) such as complex impedance (Z^*), complex permittivity (ε^*) and complex modulus (M^*) are used [17–20].

Complex real and imaginary parts of impedance expressed as:

$$Z^*(\omega) = Z'(\omega) + iZ''(\omega) \quad (1)$$

where $Z' = |Z|\cos\theta and Z'' = |Z|\sin\theta$

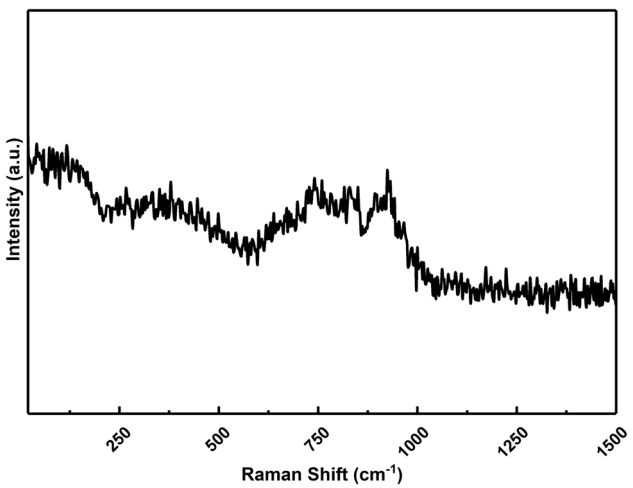

Fig. 3 Phonon modes of $10PbTiO_3$–$10Fe_2O_3$–$30V_2O_5$–$50B_2O_3$ glass obtained by Raman

Complex permittivity expressed as :

$$\varepsilon^*(\omega) = \varepsilon'(\omega) - i\varepsilon''(\omega) \quad (2)$$

The capacitive nature of the material $\varepsilon'(\omega)$ is the dielectric constant or relative permittivity while imaginary part $\varepsilon''(\omega)$ represents the loss factor, the energy required for molecular motion.

Complex real and imaginary parts of *dielectric* modulus expressed as:

$$M^*(\omega) = M'(\omega) + iM''(\omega) \quad (3)$$

$$M'(\omega) = \frac{\varepsilon'(\omega)}{\varepsilon'^2(\omega) + \varepsilon''^2(\omega)} \quad (4)$$

$$M''(\omega) = \frac{\varepsilon''(\omega)}{\varepsilon'^2(\omega) + \varepsilon''^2(\omega)} \quad (5)$$

$M''(\omega)$ is the imaginary part of the electrical modulus, which reveals the maximum asymmetric at frequency disclosing maximum loss of conduction.

The three complex dielectric electrical quantities related to each other by:

$$M^*(\omega) = \frac{1}{\varepsilon^*} = i\omega C_O Z^* \quad (6)$$

$$\tan\delta = -\frac{Z'}{Z''} = \frac{M'}{M''} = \frac{\varepsilon''}{\varepsilon'} \quad (7)$$

To investigate the mechanism of charge transport in materials the electrical conductivity dependence on temperature is carried out. The AC conductivity $\sigma_{ac}(\omega, T)$ dependence on frequency at fixed temperature can be expressed by universal power law behavior called Jonscher's law [21–23]:

$$\sigma_{ac}(\omega) = A\omega^s \quad (8)$$

$$\sigma(\omega, T) = \sigma_{dc}(T) + A(T)\omega^{S(T)} \quad (9)$$

where $\sigma(\omega, T)$ is the total measured conductivity, and σ_{dc} is the direct current conductivity. The frequency exponent S(T) is temperature dependent and varies from 0 to 1.

Using the dielectric loss values, the ac conductivity of all samples can be calculated according to the following relation [24]:

$$\sigma^*(\omega) = \sigma'(\omega) + i\sigma''(\omega) \quad (10)$$

$$\sigma^*(\omega) = i\epsilon_o\omega\epsilon^*(\omega) = i\epsilon_o\omega(\epsilon' - i\epsilon'') \quad (11)$$

From the real part (loss factor), the ac conductivity can be expressed as:

$$\sigma_{ac}(\omega) = \epsilon_o\omega\epsilon'' \quad (12)$$

The diffusivity degree can be quantified by the modified Curie–Weiss law as:

$$\frac{1}{\epsilon'} - \frac{1}{\epsilon'_{max}} = \frac{(T - T_{max})^\gamma}{C},\ 1 \le \gamma \le 2\ and\ T > T_m \quad (13)$$

where C is the Curie constant and γ is the diffuseness degree.

Under applying AC field, the relaxation in dielectric spectroscopy is related to dipole moment orientation in materials. The materials behavior depending on the frequency and temperatures. The dielectric constant $\varepsilon'(\omega)$, the capacitive nature of the material, behavior is different for polar and non-polar materials. For non-polar materials $\varepsilon'(\omega)$ is independent on temperature while it increases with temperature for polar one. The dielectric constant of the quenched $10PbTiO_3$–$10Fe_2O_3$–$30V_2O_5$–$50B_2O_3$ glass is investigated with increasing temperature and fixed frequencies, Fig. 4. The values of dielectric constant $\varepsilon'(\omega)$ decrease with increasing frequency while broad peak observed with temperature increasing. As the frequency increases the $\varepsilon'(\omega)$ peak shifted to the higher temperatures and the broadening decreases.

The origin of this peak is related to the relaxor behavior due to the existence of distorted perovskite lead titanate and/or fine polar nanoclusters in glass matrix, as explained using DSC, TEM [24] and Raman results. The dielectric loss tangent (tanδ) also, confirms the similar frequency dependent behavior of relaxor, Fig. 5. The same behavior was observed in barium titanate-doped glass [5, 6], $Pb(Sc_{1/2}Nb_{1/2})O_3$ ceramic system [25]. At low temperatures, the dipole molecules cannot orient themselves, whereas higher temperatures facilitating dipole orientation. At lower frequencies of Fig. 5, the higher values of dielectric constant could be related to space charge relaxation due to charge carriers at the interface between the samples and electrodes, interfacial polarization. The DSC curve shows two endothermic peaks nearly at the same temperature, Curie's temperature (T_c) (401 and 437 K) as of the dielectric constant peaks which support the idea of relaxor ferroelectrics phase formation and/or ferroelectric to paraelectric phase transition.

The complex dielectric modulus, M^*, is given by the inverse of complex dielectric constant ε^* where the dielectric modulus represents the real dielectric relaxation process [24]. M'(ω) and M''(ω) can be calculated from Eqs. 4, 5, 6. Figure 6 displays the

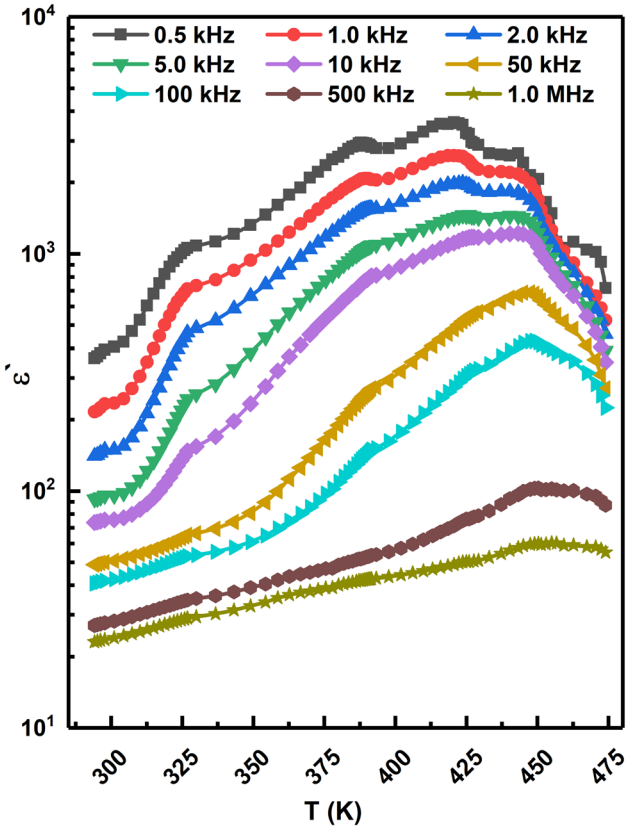

Fig. 4 Dielectric constant $\varepsilon'(\omega)$ as a function of temperatures at fixed frequencies of $10PbTiO_3$–$10Fe_2O_3$–$30V_2O_5$–$50B_2O_3$ glass

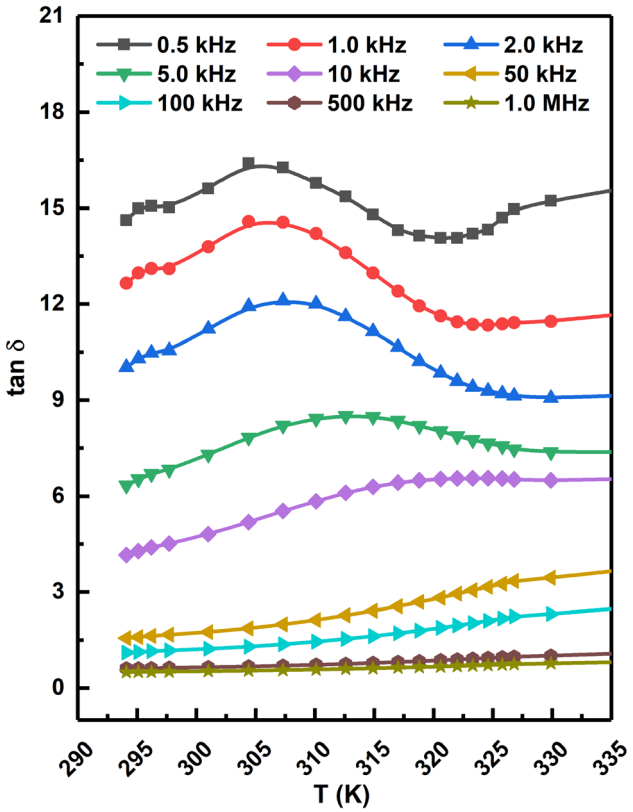

Fig. 5 Dielectric loss tangent (tan δ) as a function of temperatures at fixed frequencies of $10PbTiO_3$–$10Fe_2O_3$–$30V_2O_5$–$50B_2O_3$ glass

variation of $M'(\omega)$ and $M''(\omega)$ as a function of frequencies at different temperature. Generally, $M'(\omega)$ and $M''(\omega)$ decreases with increasing temperature while increases with frequency increases. At higher temperature $M'(\omega)$ and $M''(\omega)$ tends to have a constant value. The real and imaginary parts of dielectric modulus position shift towards the higher frequency. This indicating the presence of dielectric relaxation, which is thermally activated, in which the hopping process of charge carriers is predominant. Figure 7 shows dependence of imaginary part of electric modulus $M''(\omega)$ on the real part $M'(\omega)$ at fixed temperature, Cole–Cole diagram.

With increasing frequency, the maximum of dielectric constant and corresponding temperature shifts to the higher values which indicating a typical dielectric relaxor behavior. Modified Curie-Weiss law describe the dielectric constant of relaxor ferroelectrics with respect to temperature. Using Eq. (13), the diffusion coefficient "γ" can be calculated from the linear relationship obtained by plotting $\ln(T-T_{max})$ versus $\ln(1/\varepsilon'-1/\varepsilon'_{max})$ at 100 kHz is shown in Fig. 8. The value obtained for the diffusion coefficient is 1.34 at 100 kHz, which reflect the relaxation degree of ferroelectric materials. Normal ferroelectrics shows a diffusion coefficient value equal one, while in an ideal relaxor ferroelectric it is equal two [26].

3.3 Ferroelectric and ferromagnetism properties

Dielectric materials recoverable energy storage density (W_r) under applied electric field (E) can be calculated from the maximum (P_{max}) and remnant (P_r) polarization according to the following equation [27]:

$$W_r = \int_{P_r}^{P_{max}} EdP \tag{14}$$

Also, from the *P*–*E* curves, energy storage efficiency can be calculated as:

$$\eta = \frac{W_r}{W_r + W_{loss}} \tag{15}$$

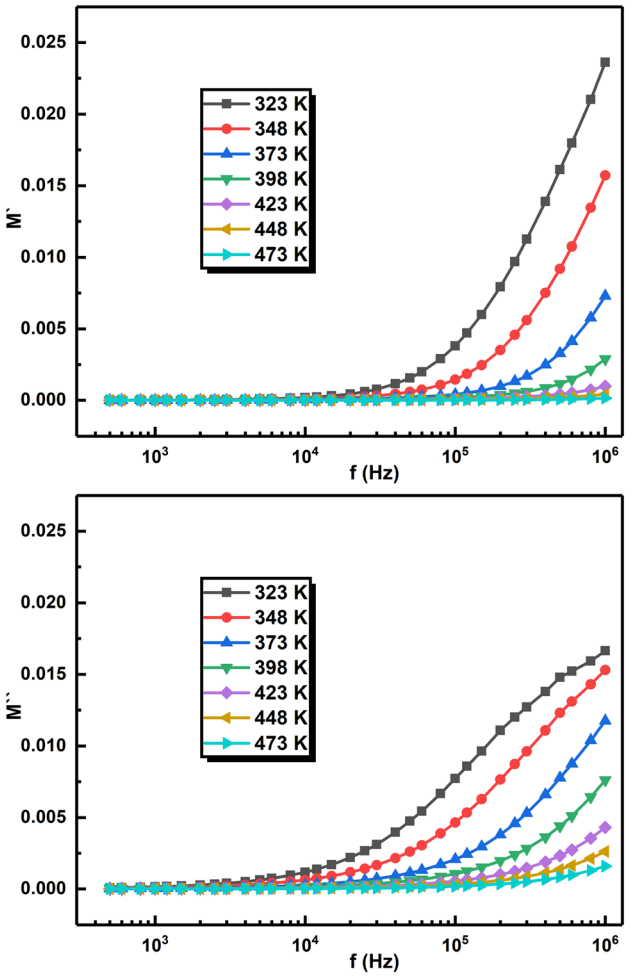

Fig. 6 Electric modulus $M'(\omega)$ and $M''(\omega)$ versus frequency at fixed temperatures of $10PbTiO_3$–$10Fe_2O_3$–$30V_2O_5$–$50B_2O_3$ glass

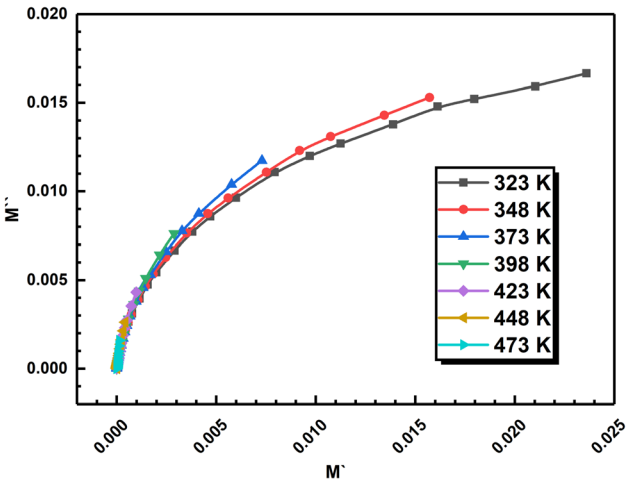

Fig. 7 Real $M'(\omega)$ and imaginary $M''(\omega)$ parts dependance of electric modulus at fixed temperatures of $10PbTiO_3$–$10Fe_2O_3$–$30V_2O_5$–$50B_2O_3$ glass

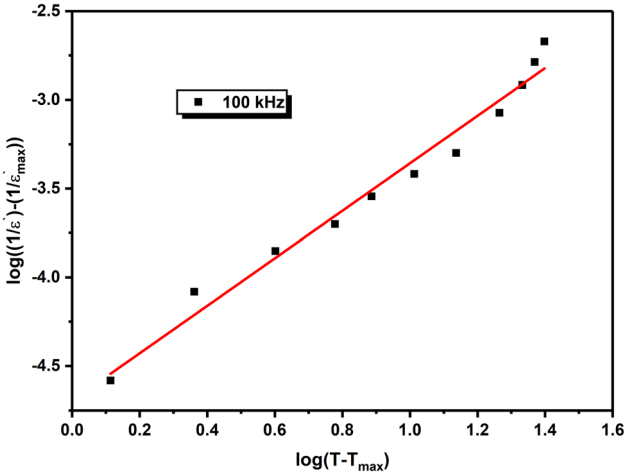

Fig. 8 $\log(T-T_{max})$ versus $\log(1/\varepsilon'-1/\varepsilon'_{max})$ at 100 kHz of $10PbTiO_3$–$10Fe_2O_3$–$30V_2O_5$–$50B_2O_3$ glass

The ferroelectric properties of $10PbTiO_3$–$10Fe_2O_3$–$30V_2O_5$–$50B_2O_3$ glass were revealed by polarization–electric field hysteresis loop measured at different temperature as displayed in Fig. 9. Ferroelectric like shaped hysteresis loop was observed at 303 K, which is related to relaxors ferroelectric nanoregions. With increasing temperature, the hysteresis loop become narrower and centered due to intermediate range polar phase decreases, slim loop. According to Eqs. (14 and 15), recoverable energy storage density (W_r) can be calculated values from the integrated area within the P–E loops. With increasing temperature remnant polarization (P_r) and coercive field (E_c) decreases while recoverable energy storage density and energy storage efficiency (η) increases, Fig. 10. The related ferroelectric parameters are summarized in Table 1. The higher values of W_r and η were observed with higher values of ΔP (difference between maximum polarization and remnant polarization). Its concluded that [6, 27], polar clusters of distorted lead titanate existence in glass matrix can be used for energy storage applications due to high dielectric constant and high energy storage density. As a weak polar structure, relaxor ferroelectrics in polar nanoregions is more sensitive to the external electric field. Often small values of P_r and significant increase in P_{max} which is consistent with their dielectric constant. This phenomenon is related to the distortion of the octahedral [TiO_6] [5, 6]. Figure 11 shows the as–quenched glass magnetization curve. Linear trend as for typical anti-ferromagnetic state, no hysteresis was found. As it is known, Hematite

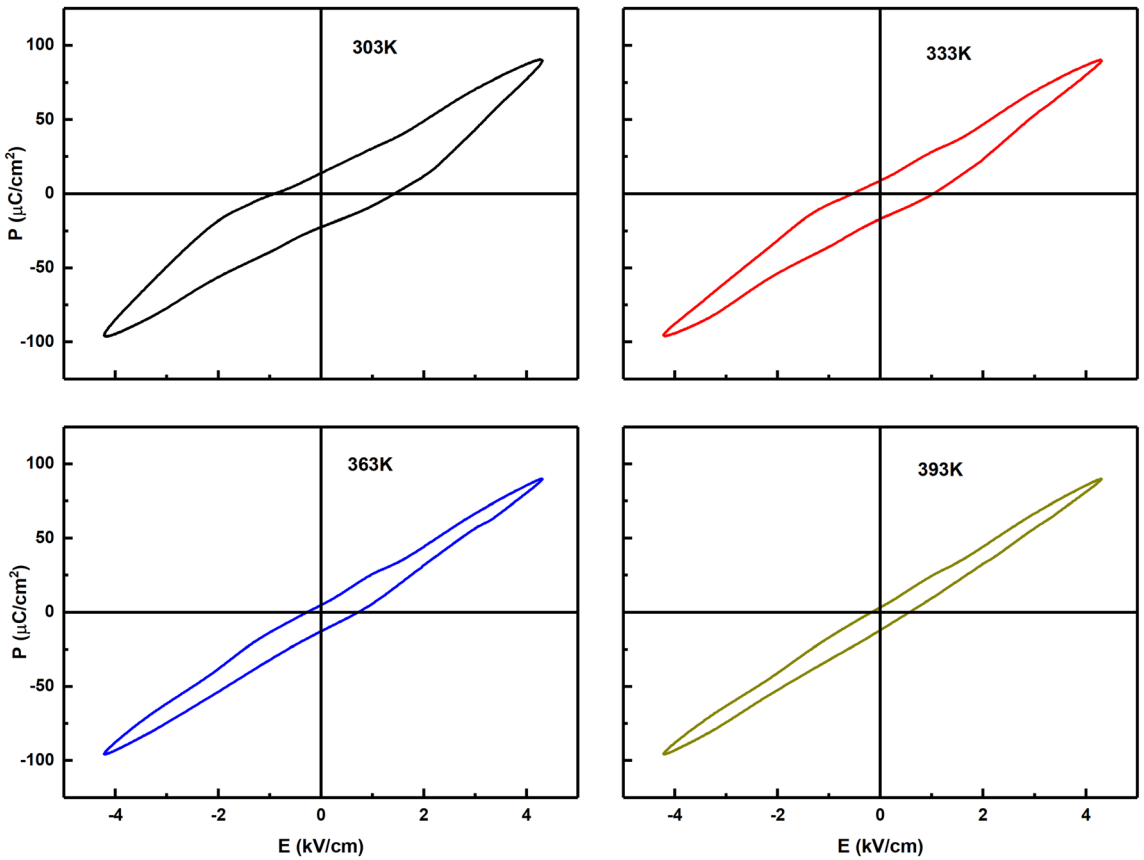

Fig. 9 P – E hysteresis loop obtained by a Sawyer–Tower Bridge

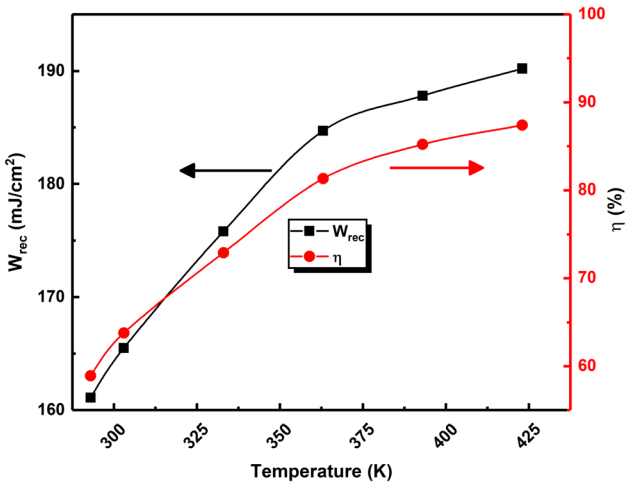

Fig. 10 Temperature dependence of energy storage properties for$10PbTiO_3–10Fe_2O_3–30V_2O_5–50B_2O_3$ glass

has anti-ferromagnetic below its Néel temperature ≈ 955 K [28, 29]. The magnetic properties of the present system required more investigation in separate work.

4 Conclusion

(1) $10PbTiO_3–10Fe_2O_3–30V_2O_5–50B_2O_3$ glass was successfully prepared by the conventional quenching method.
(2) The glassy nature was confirmed by XRD and DSC measurements.
(3) Relaxor/ferroelectric behavior appeared in quenched glass system due to polar clusters embedded in the glass matrix.
(4) DSC, Raman and frequency dependent dielectric measurements confirm Relaxor/ferroelectric formation.
(5) Recoverable energy storage density increased from 164.7 to 230.8 mJ/cm^3 with increasing temperature from 303 to 393 K which could be considered for energy storage applications.
(6) Quenched glass system obtained, exhibit anti-ferromagnetic behavior at room temperature.

Table 1 Ferroelectric parameters of $10PbTiO_3$–$10Fe_2O_3$–$30V_2O_5$–$50B_2O_3$ glass with temperature

Temperature (K)	293	303	333	363	393	423
E_c (kV/cm)	1.73	1.42	1.01	0.75	0.56	0.48
P_r (μC/cm^2)	15.84	13.79	8.89	4.42	3.11	2.26
P_r/P_{max}	0.174	0.151	0.098	0.049	0.034	0.025
$\Delta P = P_{max} - P_r$	75.1	77.2	82.1	86.5	87.8	88.7
W_r (mJ/cm^3)	161.1	165.5	175.8	184.7	187.8	190.2
W_{loss} (mJ/cm^3)	112.6	94.1	65.2	42.6	32.7	27.5
η (%)	58.9	63.8	72.9	81.3	85.2	87.4

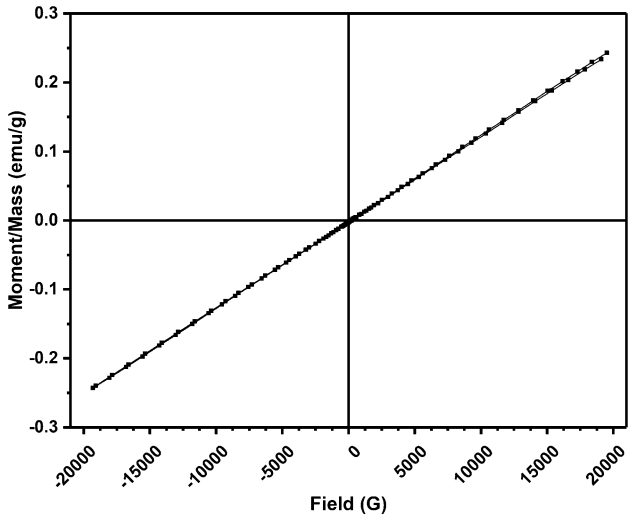

Fig. 11 Magnetization curve of $10PbTiO_3$–$10Fe_2O_3$–$30V_2O_5$–$50B_2O_3$ glass

Acknowledgements

This Project was supported financially by the Academy of Scientific Research and Technology (ASRT), Egypt Grant No. 6365 Science UP/ASRT.

Declarations

Conflict of interest The authors declare that they have no known competing financial interests or personal relationships that could have appeared to influence the work reported in this paper. The authors declare that no financial interests/personal relationships which may be considered as potential competing interests.

References

1. A.A. Bokov, Z.-G. Ye, Dielectric relaxation in relaxor ferroelectrics. J. Adv. Dielectr. **02**(02), 1241010 (2012)
2. R.A. Cowley, S.N. Gvasaliya, S.G. Lushnikov, B. Roessli, G.M. Rotaru, Relaxing with relaxors: a review of relaxor ferroelectrics. Adv. Phys. **60**(2), 229–327 (2011)
3. L.E. Cross, Relaxor ferroelectrics. Ferroelectrics **76**(1), 241–267 (1987)
4. W. Kleemann, S. Miga, J. Dec, J. Zhai, Crossover from ferroelectric to relaxor and cluster glass in $BaTi_1 - xZrxO_3$ (x = 0.25–0.35) studied by non-linear permittivity. Appl. Phys. Lett. **102**(23), 232907 (2013)
5. M.M. El-Desoky, A.E. Harby, A.E. Hannora, M.S. Al-Assiri, Relaxor Ferroelectric-Like Behavior in Barium Titanate-Doped Glass via Formation of Polar Clusters. J. Cluster Sci. **28**(4), 2147–2156 (2017)
6. A.E. Harby, A.E. Hannora, M.M. El-Desoky, Observation of relaxor-like behavior in BT and PT doped glasses for energy storage applications. J. Alloy. Compd. **770**, 906–913 (2019)
7. T.K. Pietrzak, Multi-device software for impedance spectroscopy measurements with stabilization in low and high temperature ranges working under Linux environment. Ionics **25**(5), 2445–2452 (2019)
8. T.K.J. Pietrzak, E. Wasiucionek, M. Nowiński, Nanocrystallisation in vanadate phosphate and lithium iron vanadate phosphate glasses. Phys. Chem. Glasses-Eur. J. Glass Sci. Technol. Part B **57**(3), 113–124 (2016)
9. A.E. Hannora, M.M. El-Desoky, Effects of heat treatment on the structural and electrical conductivity of Fe_2O_3–P_2O_5–PbO glasses. J. Mater. Sci.: Mater. Electr. **30**(21), 19100–19107 (2019)
10. T.K. Pietrzak, M. Maciaszek, J.L. Nowiński, W. Ślubowska, S. Ferrari, P. Mustarelli, M. Wasiucionek, M. Wzorek, J.E. Garbarczyk, Electrical properties of V_2O_5 nanomaterials prepared by twin rollers technique. Solid State Ionics **225**, 658–662 (2012)
11. A.A. Bahgat, B.A.A. Makram, E.E. Shaisha, M.M. El-Desoky, Ferroelectricity in the glassy material of the composition Bi_2O_3–Pb_3O_4–CuO–K_2O. J. Alloy. Compd. **506**(1), 141–150 (2010)
12. E. Stavrou, C. Tsiantos, R.D. Tsopouridou, S. Kripotou, A.G. Kontos, C. Raptis, B. Capoen, M. Bouazaoui, S. Turrell, S. Khatir, Raman scattering boson peak and differential

scanning calorimetry studies of the glass transition in tellurium–zinc oxide glasses. J. Phys.: Condens. Matter. **22**(19), 195103 (2010)
13. J. Schroeder, W. Wu, J.L. Apkarian, M. Lee, L.-G. Hwa, C.T. Moynihan, Raman scattering and Boson peaks in glasses: temperature and pressure effects. J. Non-Cryst. Solids **349**, 88–97 (2004)
14. V.K. Malinovsky, A.P. Sokolov, The nature of boson peak in Raman scattering in glasses. Solid State Commun. **57**(9), 757–761 (1986)
15. T. Nakamura, M. Takashige, H. Terauchi, Y. Miura, W.N. Lawless, The Structural, Dielectric, Raman-Spectral and Low-Temperature Properties of Amorphous $PbTiO_3$. Jpn. J. Appl. Phys. **23**(Part 1), 1265–1273 (1984) No. 10)
16. A.E. Hannora, M.A. Abbas, M.M. El-Desoky, Annealing effects on the structural, thermal, and electrical properties of 10PbTiO3–10Fe2O3–30V_2O_5–50B_2O_3 glass. J. Mater. Sci.: Mater. Electr. **32**(4), 3998–4007 (2021)
17. B.M. Tareev, *Physics of Dielectric Materials* (Mir Publishers, Moscow, 1975)
18. A.K. Behera, N.K. Mohanty, B. Behera, P. Nayak, Impedance properties Of 0.7($BiFeO_3$)-0.3 ($PbTiO_3$) composite. Adv. Mater. Lett. **4**(2), 141–145 (2013)
19. A. Edukondalu, N. Venkatesham, D. Keerthi Devi, S. Rahman, K. Siva Kumar, AC conductivity and dielectric properties of B_2O_3-WO_3-TeO_2- Li_2O glasses. Mater. Today: Proc. **5**(13, Pt 1), 26232–26237 (2018)
20. S. Türkay, A. Tataroğlu, Complex dielectric permittivity, electric modulus and electrical conductivity analysis of Au/Si_3N_4/p-GaAs (MOS) capacitor. J. Mater. Sci.: Mater. Electron. **32**(9), 11418–11425 (2021)
21. A.K. Jonscher, The 'universal' dielectric response. Nature **267**(5613), 673–679 (1977)
22. Y.J. Wong, J. Hassan, M. Hashim, Dielectric properties, impedance analysis and modulus behavior of $CaTiO_3$ ceramic prepared by solid state reaction. J. Alloy. Compd. **571**, 138–144 (2013)
23. A.R. Long, Frequency-dependent loss in amorphous semiconductors. Adv. Phys. **31**(5), 553–637 (1982)
24. A. Eroğlu, A. Tataroğlu, Ş Altındal, On the temperature dependent dielectric properties, conductivity and resistivity of MIS structures at 1 MHz. Microelectron. Eng. **91**, 154–158 (2012)
25. F. Chu, I.M. Reaney, N. Setter, Spontaneous (zero-field) relaxor–to–ferroelectric-phase transition in disordered Pb(Sc1/2Nb1/2)O_3. J. Appl. Phys. **77**(4), 1671–1676 (1995)
26. X. Li, Z. Wang, Y. Liu, C. He, X. Long, A new ternary ferroelectric crystal of Pb(Y1/2Nb1/2)O_3–Pb(Mg1/3Nb2/3)O_3–$PbTiO_3$. CrystEngComm **16**(32), 7552–7557 (2014)
27. N. Sun, Y. Li, X. Liu, X. Hao, High energy-storage density under low electric field in lead-free relaxor ferroelectric film based on synergistic effect of multiple polar structures. J. Power Sources **448**, 227457 (2020)
28. J.B. Lee, H.J. Kim, J. Lužnik, A. Jelen, D. Pajić, M. Wencka, Z. Jagličić, A. Meden, J. Dolinšek, Synthesis and magnetic properties of hematite particles in a "Nanomedusa" morphology. J. Nanomater. **2014**, 902968 (2014)
29. F. Bødker, M.F. Hansen, C.B. Koch, K. Lefmann, S. Mørup, Magnetic properties of hematite nanoparticles. Phys. Rev. B **61**(10), 6826–6838 (2000)